Internal dynamics and ionization states of the macrophage migration inhibitory factor: Comparison between wild-type and mutant forms

ARTICLE *in* BIOPOLYMERS · NOVEMBER 2002

Impact Factor: 2.39 · DOI: 10.1002/bip.10252 · Source: PubMed

4 AUTHORS, INCLUDING:

Thereza A Soares
Federal University of Pernambuco
53 PUBLICATIONS **820** CITATIONS
SEE PROFILE

Roberto D Lins
Oswaldo Cruz Foundation, Recife, Brazil
59 PUBLICATIONS **1,463** CITATIONS
SEE PROFILE

James M Briggs
University of Houston
95 PUBLICATIONS **4,148** CITATIONS
SEE PROFILE

T. A. Soares[1]
R. D. Lins[1]
T. P. Straatsma[2]
J. M. Briggs[3]
[1] *Laboratory of Physical Chemistry, Swiss Federal Institute of Technology, Zurich, Switzerland*

[2] *Environmental Molecular Sciences Laboratory, Pacific Northwest National Laboratory, Richland, WA 99352, USA*

[3] *Department of Biology and Biochemistry, University of Houston, Houston, TX 77204-5001, USA*

Received 25 April 2002; accepted 10 July 2002

Internal Dynamics and Ionization States of the Macrophage Migration Inhibitory Factor: Comparison Between Wild-Type and Mutant Forms

Abstract: *The macrophage migration inhibitory factor (MIF) is a cytokine that shares a common structural architecture and catalytic strategy with three isomerases: 4-oxalocrotonate tautomerase, 5-carboxymethyl-2-hydroxymuconate isomerase, and D-dopachrome tautomerase. A highly conserved N-terminal proline acts as a base-acid during the proton transfer reaction catalyzed by these enzymes. Such unusual catalytic strategy appears to be possible only due to the N-terminal proline pK_a shifted to 5.0–6.0 units. Mutations of this residue result in a significant decrease of the catalytic activity of MIF. Two hypotheses have been proposed to explain the catalytic inefficiency of MIF: the lower basicity of primary amines with regard to secondary ones and the increased flexibility resulting from the replacement of a proline by residues like glycine. To investigate that, we have performed molecular dynamics simulations of MIF wild-type and its mutant P1G, as well as calculated the protonation properties of several mutant forms. It was found that the N-terminal glycine does not show larger fluctuations compared to proline, but the former residue is more exposed to the solvent throughout the simulations. The apparent pK_a of these residues displays very little change (as expected from the structural rigidity of MIF) and is not significantly affected by the surrounding ionizable residues. Instead, the hydrophobic character of the active site seems to be the*

Correspondence to: T. A. Soares at Läboratorium für Physikalische Chemie, ETH Hönggerberg, HCI G223. CH-8093 Zürich, Switzerland; email: tsoares@igc.phys.chem.ethz.ch

Contract grant sponsor: National Institutes of Health

Biopolymers, Vol. 65, 313–323 (2002)

main factor in determining the pKa of the N-terminal residue and the catalytic efficiency of MIF.

Keywords: *molecular dynamics; Poisson–Boltzmann electrostatics; catalytic mechanism*

INTRODUCTION

The macrophage migration inhibitory factor (MIF) is a cytokine that activates neutrophils, macrophages and T-cells.[1,2] MIF is released as a hormone by the anterior pituitary gland and activated T-lymphocytes in response to a diversity of proinflammatory stimuli.[3–5] Once released, MIF has the potential to counterregulate the immunosuppressive effect of glucocorticoids on macrophage cytokine production and on lipopolysaccharide-induced lethality.[5,6] Besides playing the role of cytokine in a broad range of immunoregulatory activities, MIF also catalyzes chemical reactions acting as a D-dopachrome tautomerase[7] and a phenylpyruvate tautomerase.[8] Crystallographic studies have shown that MIF does not share a common structural architecture with other known cytokines, but with three other isomerases: 4-oxalocrotonate tautomerase (4OT), 5-carboxymethyl-2-hydroxymuconate isomerase (CHMI), and D-dopachrome tautomerase (DDT)[9] (Figure 1). MIF is a trimer of identical subunits where each monomer contains two antiparallel α-helices packed against a four-strand β-sheet[10] (Figure 1). Two β-strands of each monomer interact with the β-sheets of the adjacent monomers, forming the interface between MIF subunits. The β-sheets are arranged in a barrel fashion, forming a solvent-accessible channel along the molecular 3-fold axis in the center of the structure. The three active sites are located between the interfaces constituted by adjacent pairs of monomers. Although the sequence alignment between MIF and the isomerases reveals low homology, a highly conserved N-terminal proline has been observed in all of them.[11] This proline has been implicated in the biochemical reactions catalyzed by MIF and these isomerases.[12] In addition, they share an unusual catalytic strategy of proton transfer in which the N-terminal proline acts as a base as its pK_a is shifted from about 9.4, typical of an isolated proline, to that of 6.0–6.4 in the MIF protein.[13,14]

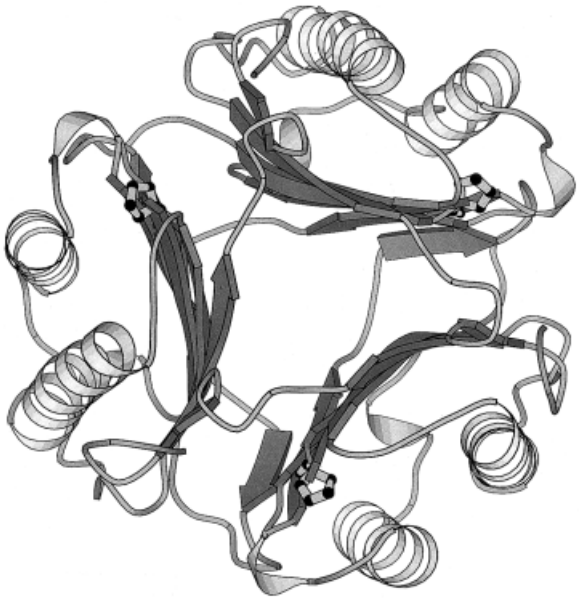

FIGURE 1 Cartoon representation of three-dimensional structure of macrophage migration inhibitory factor. The active sites are indicated by N-terminal proline residues in stick model.

Although mutational studies have established that the N-terminal proline is required for the isomerase–tautomerase activities of MIF,[14–16] its actual role in the enzymatic reaction is still a matter of debate. It has been suggested that the N-terminal proline acts as a general base in phenylpyruvate tautomerase[14] and D-dopachrome tautomerase activities.[17] More recently, this proline has been proposed to function as both general acid and base catalysts in phenylpyruvate tautomerase activity.[18] Such function does not appear to hold for D-dopachrome tautomerase activity since the protonation/deprotonation sites are spatially separated so as to require only one residue to act as a general acid.[17]

The significance of MIF's catalytic activity to its physiological function is not clear. D-Dopachrome is not found in biological systems and reported values of the Michaelis–Menten constant (K_M) for phenylpyruvate and *p*-(hydroxyphenyl)pyruvate are too high for these molecules to be physiological substrates,[8] making it unlikely that these are the biological substrates of MIF. Recently, new insight has emerged from the discovery that MIF converts toxic quinone products of the neurotransmitter catecholamines into hydroxyindole derivatives, precursors of neuromelanin.[19] These findings indicate that the enzymatic activity of MIF may play a role in a detoxification pathway for catecholamine products, which is supported by the high level of MIF in neural tissues.[19] Therefore MIF would be a potential target for the treatment of catecholamine-related diseases, such as Parkinson's disease.

EXPERIMENTAL BACKGROUND: RIGIDITY VS pK_a

Determinations of kinetic properties of mutant forms of MIF indicate that the major effects of replacing a rigid secondary amine (Pro) with a more flexible primary amine (Gly) are on the values of k_{cat} and k_{cat}/K_M.[18,20] The mutation P1G has no effect on K_M, but decreases k_{cat} from ca. 680 to ca. 200-fold depending on the substrate.[18] As a result, a reduction of 230–200-fold in k_{cat}/K_M can be observed.[18] On the basis of the Brønsted relationship, it has been suggested that such a decrease in catalysis may be due to the lower basicity of primary amines. However, it has been argued that assuming a difference in pK_a between Pro and Gly at the active site of 0.8 pK_a units, the lower basicity of Gly1 does not fully account for the decrease in k_{cat}.[20] Therefore, it has been reasoned that the increased flexibility resulting from the replacement of a proline by a glycine can account for the decrease in the catalytic efficiency of the P1G mutant.[20]

It is worth noting that MIF, 4OT, CHMI, and DDT are the only enzymes known to employ a N-terminal proline as general acid/base. The identification of the molecular properties that make an N-terminal proline suitable to act as a catalyst is an important step in the characterization of reaction mechanisms exhibited by this new superfamily of enzymes. It is also expected to bring insights into the design of structure-based inhibitors. In this context, we have performed molecular dynamics simulations for the wild-type (MIF-wt) and a mutant form (MIF-P1G) of MIF, and estimated the ionization states of residues in MIF-wt and several mutant forms. These simulations are expected to better depict the relationship between rigidity and pK_a in shaping the ability of Pro1 to act as a catalyst.

METHODOLOGY

MD simulations were performed using the x-ray structure of the macrophage migration inhibitory factor corresponding to the Protein Data Bank entry 1MIF.[10] 1MIF is a homotrimer, each monomer consisting of 115 residues, solved to a resolution of 2.6 Å. The mutant form was generated by mutation of all three N-terminal Pro into Gly residues using the Insightll program. Coordinates for hydrogen atoms were generated using the prepare module of NWChem v3.1 program,[21] based on the predicted ionization state for each residue using the pK_a procedure[22,23] as implemented in the UHBD program.[24,25] The N-terminal proline and glycine reśidues were taken in their protonated states, according to the experimental pK_a data available.[14,20] Water molecules were added around the protein within a cube with dimensions of 7.4 $\times$ 7.4 $\times$ 7.4 nm. The MIF-wt and MIF-P1G systems achieved overall neutrality with the addition of 3 Mg^{2+} ions, resulting in a total number of solute/solvent atoms equal to 5169/34362 and 5148/34359, respectively. The SPC/E water model[26] was used to describe the solvent atoms. A short-range cutoff of 1.0 nm was used for all nonbonded interactions while long-range electrostatic interactions were treated by the particle-mesh-ewald (PME) method (64^3 grid). The bond lengths between hydrogen and heavy atoms were constrained using the SHAKE algorithm[27] with a tolerance of 10^{-4} nm.

Equilibration of the solute was performed by molecular dynamics for 20 ps each at temperature intervals of 50, 100, 150, 200, 250, and 298 K with velocity reassignment every 1 ps, using a 1 fs time step. Finally, the whole system (solute + solvent) was equilibrated for 100 ps at 298 K, again using a 1 fs time step. A time step of 2 fs was used during the MD simulation. Data production was carried out for the last 900 ps at 298 K under constant number of particles, pressure and temperature (NPT conditions) ($P = 1.025 \times 10^5$ Pa). Such a time scale is validated by NMR studies which show that MIF-wt exists as a rigid structure on the nanosecond time scale.[28] The temperature of solute and solvent was controlled by separately coupling them to a Berendsen thermostat with a relaxation time of 0.1 ps. Snapshots of the trajectory were recorded every 100 steps. All energy and molecular dynamics calculations were performed using the AMBER95 force field[29] and the leapfrog algorithm as implemented in the parallel NWChem v3.1 program.[21] Calculations were carried out on the Cray T3E parallel computers of the San Diego Supercomputer Center.

The solvent-accessible surfaces were calculated using Lee and Richards algorithm[30] as implemented in the Whatlf program.[31] The solvent accessible surface is generated by the center of a probe sphere of radius of 1.4 Å representing the solvent when it rolls over the van der Waals surface.[29] All accessibility calculations use united heavy atoms, and thus neglect all of the hydrogens. The precision of the accessibility calculations depends on the number of dots on the surface, which are placed using a Fibonacci algorithm. It ensures that the dots are placed on the surface as homogeneously as possible. We have used a total of 610 dots per atom, and the expected precision is roughly 5%.[31]

The protonation equilibria of ionizable sites were predicted by the finite-difference Poisson–Boltzmann

method.[22,32] In this approach the linearized Poisson–Boltzmann equation is solved numerically by applying the finite-difference procedure as described by Warwicker and Watson.[33] The effects of ionic strength are included by a Debye–Hückel term. The single-site approach was used for the pK_a predictions in conjunction with the CHARMM v.25 polar-hydrogen force field to assign partial charges and atomic radii to the x-ray coordinates. Finite-difference Poisson–Boltzmann calculations employed four grids. A grid of size 50 × 50 × 50 with 2.5 Å spacing, two grids of dimension 15 × 15 × 15 with spacing of 1.2 and 0.75 Å and a grid of size 20 × 20 × 20 with 0.25 Å spacing were centered on each ionizable site. The solvent and protein dielectric constants were taken to be 78, 20 (x-ray structures), and 6 (MD structures), respectively.[22,23] The dielectric boundary between the inner (protein or model compound) and the outer (solvent) media was defined by the contact and reentrant surfaces (i.e., molecular surface) using a solvent probe of radius 1.4 Å , representing the size of a water molecule. The simulations were performed at a temperature of 298 K and an ionic strength of 150 m*M*.

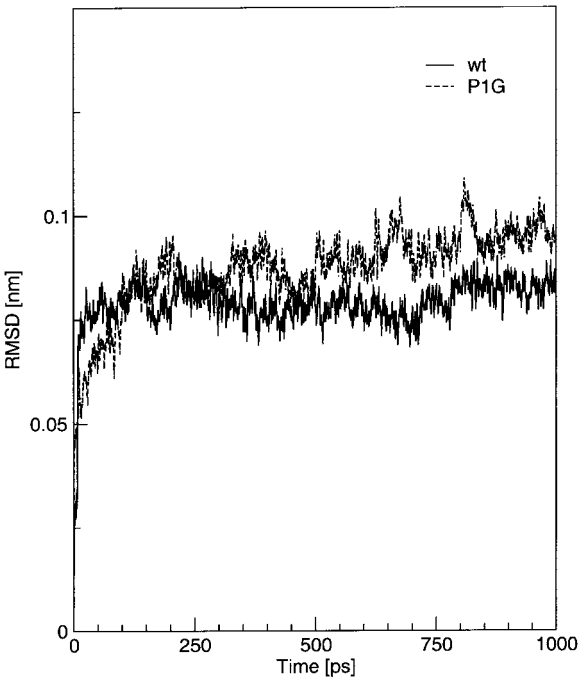

FIGURE 2 Root mean square atomic positional deviations from the x-ray structure for heavy atoms throughout the MD simulations. The wild-type (MIF-wt) is represented by the solid line and the mutant for P1G (MIF-P1G) by the dotted line.

FLEXIBILITY OF THE N-TERMINAL RESIDUES

In order to assess the flexibility of N-terminal residues in the wild-type and mutant forms of MIF, we have performed a 1 ns molecular dynamics simulation for each one of these two structures. The RMS deviations (RMSD) of all atoms from their positions in the equilibrated structures of MIF-wt and MIF-P1G remained steady during the simulations, after the initial ca. 220 ps, lingering around 0.85 and 0.95 Å, respectively (Figure 2). It points to a remarkably rigid tertiary structure, in agreement with previous NMR assignments for the wild-type form.[28] A RMSD of 0.9 Å has been observed in molecular dynamics simulations of the green fluorescent protein, which forms a cylindrical β-barrel similar to the β-barrel in MIF.[34] It has been widely recognized that barrel motifs are very rigid structural arrangements, which explains the reduced flexibility of such systems.[35] The RMS fluctuations throughout the simulation were determined and compared against crystallographic *B* factors (Figure 3). These fluctuations display a lower base level, although the overall profile of the MD data is consistent with the crystallographic *B* factors. Due to the fact that atomic *B* factors are unavailable for the x-ray structure 1MIF, we have used the values available for the x-ray structure 1MFI. These two x-ray structures can be superimposed with an RMSD equal to 0.3 Å.[28]

Further examination of atomic displacements of active site residues in MIF-wt and MIF-P1G indicates that the N-terminal residues exhibit a similar degree of vibrational motion (Figure 4). The RMS fluctuations associated with the backbone atoms of Pro1 and Gly1 are below 20 $Å^2$. That is the average value observed for backbone atoms in x-ray structures of proteins. Although these results are observed on the picoseconds time scale, they are validated by comparison to NMR studies.[28] The H^1–N^{15} heteronuclear nuclear overhauser effect (NOE) assignments indicate that MIF-wt exists as a rigid structure of very limited flexibility in the loop regions on the nanosecond to picosecond time scale.[28]

Analyses of hydrogen bonds involving Pro1 and Gly1 were performed. Two stable hydrogen-bonds have been observed, which involve the residues Pro1/Gly1 and the backbone atoms of Tyr36 and Ala38. In these interactions, the amino group of the N-terminal residues is hydrogen bonded to the carbonyl group of Tyr36 while its carbonyl group interacts with the amine group of Ala38. In the wild-type structure, the average distance between hydrogen-bond donor and acceptor atoms is on the order of 0.30–0.35 nm, and these interactions last for the entire simulation (Figure 5). In the mutant MIF-P1G simulation, the corre-

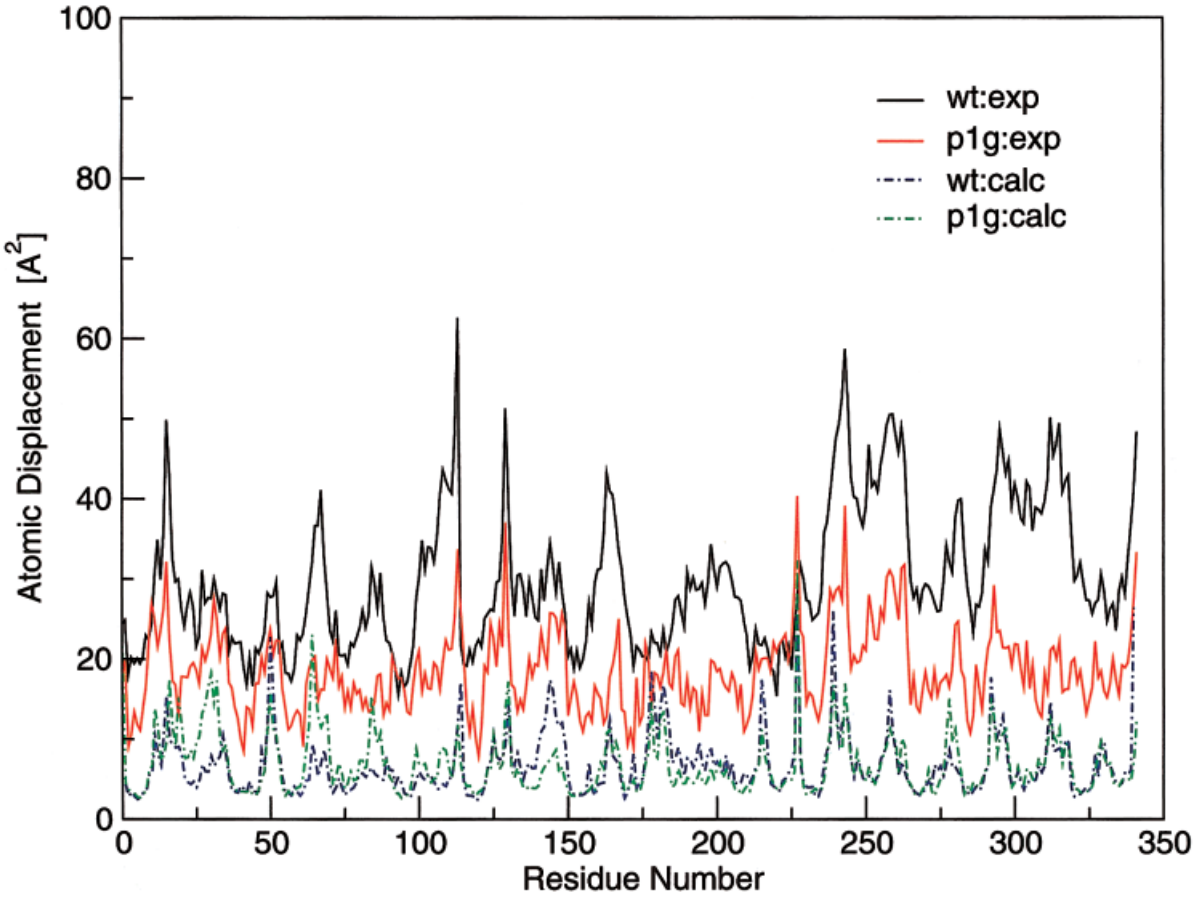

FIGURE 3 Comparison between crystallographic *B* factors and RMS atomic fluctuations for C_α atoms throughout the MD simulations of MIF-wt and MIF-P1G.

sponding hydrogen bonds are present only during the initial 600 ps of the simulation (Figure 5). Furthermore, investigation of the solvent-accessible surfaces of Pro1 and Gly1 along the MD simulation displayed a steady difference between the two structures (Figure 6). The average solvent-accessible areas of Pro1 and Gly1 in the protein are respectively 18 and 27 Å^2, in contrast with their surface areas when fully immersed in water, 74 and 57 Å^2, respectively. This difference in what refers to the protein environment seems to result from small conformational changes of residues composing the active site, which thus builds up to change the solvation pattern of the catalytic residue in the mutant protein (Figure 7).

IONIZATION STATES OF THE N-TERMINAL RESIDUE OF MIF-WT AND ITS MUTANTS

Calculations of the pH-dependent properties in proteins using the Poisson–Boltzmann model allow for certain variables such as ionic strength and dielectric constant of the solvent to be set according to the experimental conditions to be simulated. However, the dielectric constant of the protein is less certain. Several dielectric constants have been used in theoretical studies of proteins, obtained either from direct application of equations as Coulomb's law,[36,37] Tanford–Kirkwood model,[38] and generalized Poisson–Boltzmann,[33] or from a theory that establishes a link with polarizability of the system as Kirkwood–Frölich theory.[39,40] Overall, the utilization of dielectric constant is an attempt to take into account features of the system that are not treated explicitly in the calculations. In the Poisson–Boltzmann model, the protein dielectric constant implicitly represents electronic polarization and structural aspects as displacements associated with charge alterations and fluctuations. Therefore, it has been argued that in the absence of more detailed models, the dielectric constant may be considered an adjustable parameter that must be determined by comparison of theoretical and experimental data.[41]

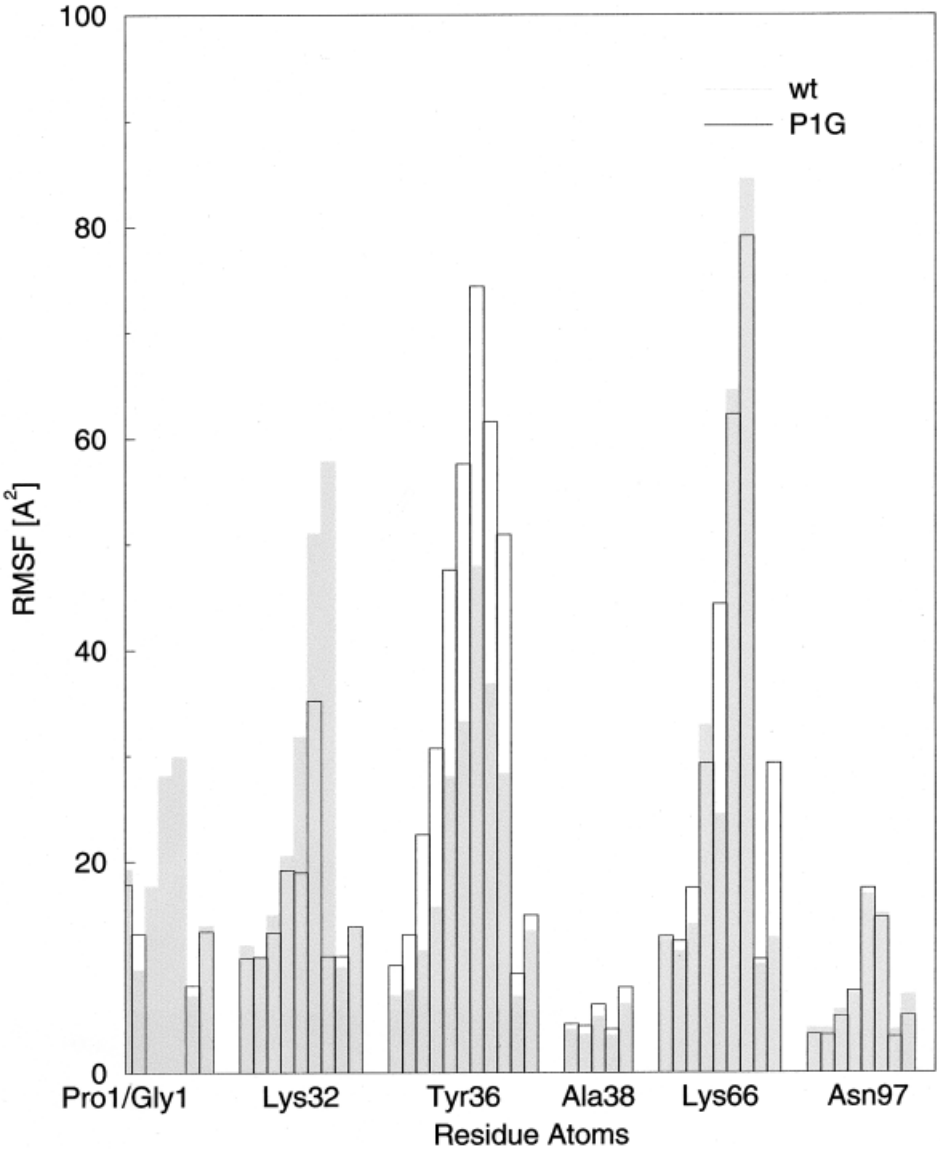

FIGURE 4 Comparison between RMS atomic fluctuations between active site residues of MIF-wt and MIF-P1G.

Previous calculations on folded proteins yield dielectric constants in the range 2–5, excluding contributions of ionized groups to the fluctuations in dipole moment of the molecule.[39,42,43] However, it has been shown that the Poisson–Boltzmann approach gives more accurate results for predicting pK_as when the interior dielectric constant is assumed to be 20 rather than the more commonly used values of 2.0–4.0.[22,23,41,44,45] Recently, Grycuk[46] has proposed to represent free amino acids (model compounds) by a minimal set of atoms necessary to describe a nonflexible group (namely, model group). Such an approach seems to minimize the effects resulting from absence of conformational flexibility on the pK_a values used as model compounds in the Poisson–Boltzmann model. When applied to hen egg lysozyme and turkey ovomucoid third domain, the model group approach suggests an optimal dielectric constant $\varepsilon_p = 12–13$.[46]

The use of a dielectric constant of 4 to calculate the ionization states for x-ray structures yielded inaccurate pK_a values (Table I). Either dielectric constants 4 or 20 failed to reproduce the experimental values when applied to the MD ensembles (data not shown). The dielectric constant of 20 resulted in pK_a values higher (more basic) than expected while the dielectric constant of 4 produced lower (more acid) pK_a values. Hence, we have calibrated the dielectric constant to the value of 6, which reproduces better the experi-

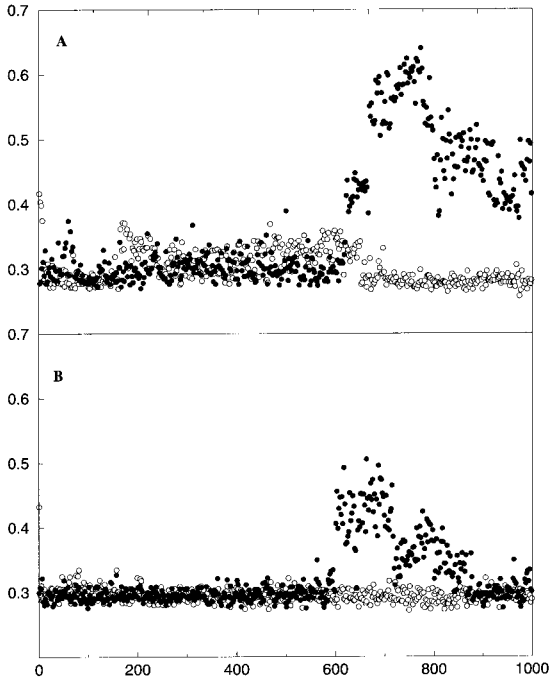

FIGURE 5 (A) Distances between the amine nitrogen and carbonyl oxygen atoms in the N-terminal residue and the carbonyl oxygen atom of Tyr36. (B) Distances between the carbonyl oxygen in the N-terminal residue and the amine nitrogen of Ala38. MIF-wt is represented by open circles and MIF-p1g by filled circles. Averages calculated over a 50-ps window.

mental data, and is in between the calculated dielectric constants for α-helices ($\varepsilon_p = 3.5$) and β-sheets ($\varepsilon_p = 10$).[39]

The pK_a values were calculated for a number of x-ray structures (Table I) as well as for different conformations of MIF-wt and MIF-P1G obtained from two independent MD simulations (Figure 8). The pK_a values presented in Table I and Figure 8 correspond to the average between the three active sites since the experimental values are macroscopic measurements that cannot be attributed to an individual N-terminal proline (Figure 1). In this way, a proper comparison between calculated and experimental pK_a values is possible. As presented in Table I, our approach reproduces the experimental values obtained for N-terminal residues of MIF and its mutants quite well.

DISCUSSION

The pK_a values were estimated for the three ionizable N-terminal groups in thirteen configurations after 220 ps (one structure every 60 ps interval) of MIF-wt and MIF-P1G. The error associated with the experimental pK_as is 0.1 unit.[14,16,47] The standard deviation corresponding to the calculated pK_as is 0.59 for MIF-wt and 0.49 for MIF-P1G. The average difference between experimental and calculated pK_as for MIF-wt is about 0.15 unit, with the highest difference value of 0.5 unit (taken the experimental value of 5.6, see Table I). The corresponding differences for MIF-P1G cannot be determined because the exact experimental pK_a of the N-terminal Gly is unknown, The fact that the pK_a values for Pro1 were consistently greater than for Gly1 indicates that a finer sampling is not necessary (Figure 8b). Their average values of 5.8 and 5.2 pK_a units, respectively, are in good agreement with the experimental data for Pro1 and the estimated value for Gly1.[14,20] Although the average difference between the two pK_as is about 0.6 units, these differences can be larger than 1.0 pK_a units along the trajectories (Figure 8b). The standard deviation corresponding to the pK_a values calculated for the two N-terminal residues are very small (0.50 and 0.55 for MIF and P1G, respectively). Because of the sensitivity of the pK_a calculations to minor structural variations, this result corroborates the root-mean-square fluctuations (RMSF) analyses indicating that the N-terminal Gly and Pro exhibit a similar flexibility (Figures 2 and 4). In contrast, Pro1 forms two persistent hydrogen bonds while the same interactions involving Gly1 are disrupted (Figure 5). The difference between hydrogen-bond patterns in the two simulations might be interpreted as indicative of a more flexible behavior of Gly with respect to Pro. However, it should be noted that the RMSF of the active site residues identifies significant fluctuations of Tyr36, rather than the N-terminal Gly, as accountable for the disruption of these interactions (Figure 4). In fact, hydrogen bonds are highly sensitive to slight changes in distance and angle between donor and acceptor, and therefore even minor fluctuations of these groups can affect the interaction without resulting in a major conformational change of the residue.

Attempts to correlate the formation and breaking of hydrogen bonds involving the N-terminal Pro and Gly with the pK_a fluctuations in the thirteen configurations sampled from the MD simulations were unsuccessful. It may be due to the fact that the groups involved in those hydrogen bonds do not have a substantial effect on the pK_as of the N-terminal residues. To clarify this point, the effect of the active site electrostatic environment over the N-terminal residues Pro and Gly were estimated. The effect can be evaluated from the difference between the apparent pK_a and the intrinsic pK_a^{int}, which corresponds to the pK_a of a given site when all the other titratable resi-

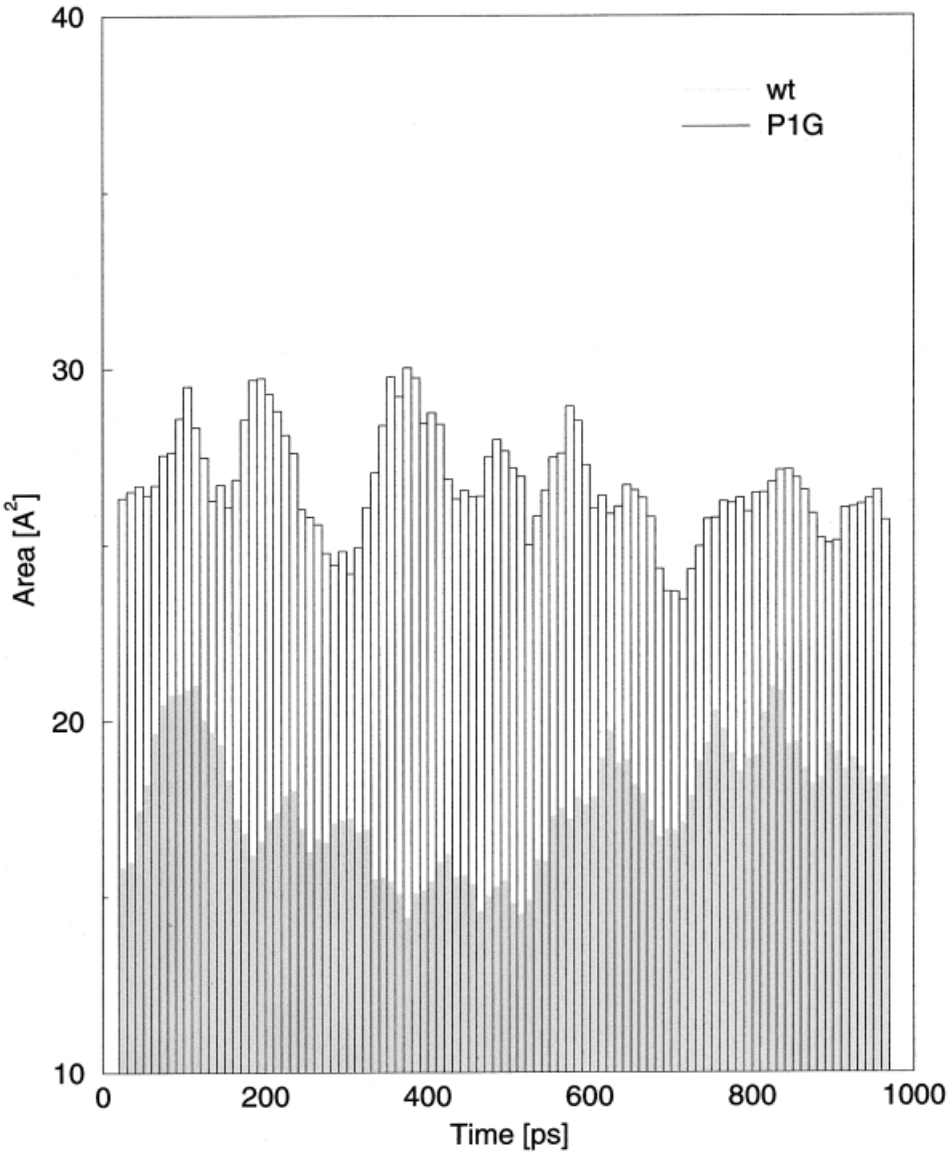

FIGURE 6 Solvent-accessible surface areas throughout the MD simulations of MIF-wt and MIF-P1G. Averages calculated over 50-ps window.

dues are in their neutral state. In other words, the shift in the pK_a^{int} is an estimate of how much the other titratable groups are contributing to the apparent pK_a of the N-terminal residue. On average, a shift of 0.50 and 0.55 pK_a units is observed for the N-terminal Pro and Gly, respectively. If it is taken into account the difference between the calculated pK_a of Pro1 and Gly1 in the protein environment and the experimentally measured pK_a of these same amino acids in the aqueous environment, it can be seen that it is about 2.0 pKa units. It is then clear that the ionizable residues in the active site play a minor role in the apparent pK_as. Among them, Lys32 and Tyr95 appear to be the most important ones given that there is no difference between the apparent and intrinsic pK_a values of the N-terminal Pro in the mutants MIF-K32A and MIF-Y95F (Table I). In a previous study, we identified Lys32 and Tyr95 as the principal ionizable residues affecting the pK_a of the N-terminal Pro.[48]

A second property that consistently differs between the two simulations is the solvent-accessible surface of Pro1 and Gly1, with an average difference of 10 $Å^2$ between them (Figure 6). In attempts to account for hydrophobic and other solvation effects, a quantity of general interest is the solvent-accessible surface.[49–51] This is because the magnitude of hydrophobicity or hydration free energy of a solute is known to be empirically linear with its water-acces-

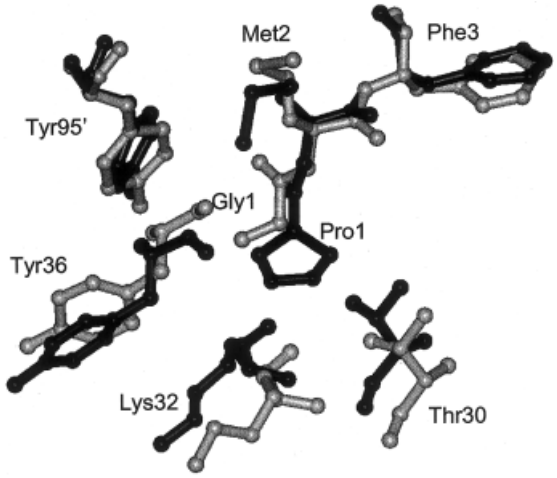

FIGURE 7 Snapshot of active site of MIF after 1.0 ns. Only residues located at the entrance of the active site pocket are displayed for clarity. In black is MIF-wt and in grey MIF-P1G. Residues belonging to the neighbor subunit are labeled by an apostrophe.

sible surface area.[52–54] Therefore, this relationship has been widely used to analyze aqueous solubility[52] water/oil partition coefficients,[55,56] and biological activity of small molecules[57] as well the unfolding and binding of proteins.[53,58,59]

In our simulations, Gly1 has an average solvent-accessible surface 1.5-fold larger that Pro1 (Figure 6), indicating that it is more exposed to the solvent. The increase of the solvent accessibility area of Gly1 results from the summation of small conformational changes in the surrounding residues, as seen in Figure 7. It has been suggested that the shifted pK_a of the N-terminal proline is a consequence of its location in a hydrophobic pocket, which lacks a neutralizing negative counter charge.[16] In that case, the higher solvent accessibility observed for Gly1 compared to Pro1 could account for the lower pK_a of Gly1. A similar effect is observed in the mutant MIF-PAM where an alanine is inserted between Pro1 and Met2. X-ray crystallography shows that this mutant displays no major structural changes as compared to the wild-type enzyme except for the displacement of Pro1 toward the solvent, which causes a decrease in its pK_a from 5.6 to 5.0.[20] Furthermore, the change in the solvation profile of Gly1 could also explain the disruption of the hydrogen bonds involving the N-terminal residue and the backbone atoms of Ala32 and Tyr36. During the MD simulations Gly1 does not show a particularly higher flexibility compared to Pro1 (Figure 4) that could rationalize the rupture of those interactions. However, the increased solvation of Gly1 exposes its amino group to interactions to the water molecules

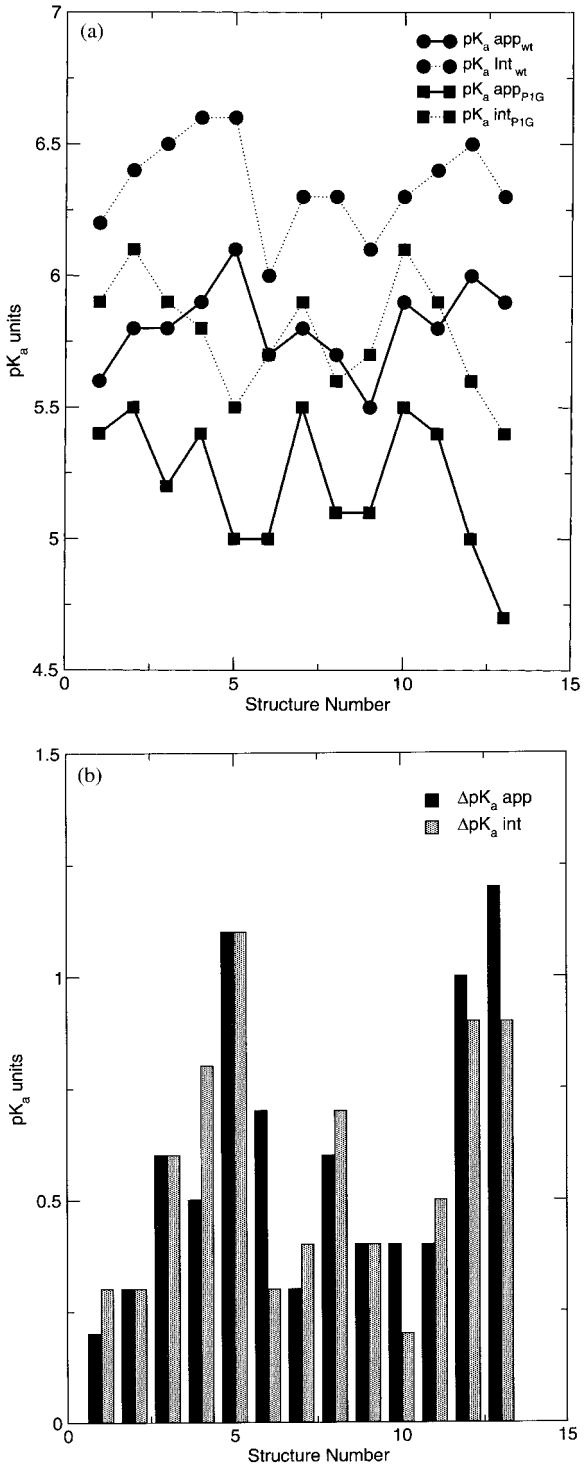

FIGURE 8 (a) Average apparent and intrinsic pK_as for Pro1 and Gly1 in thirteen MD-sampled structures of MIF-wt and MIF-P1G. (b) Relative differences of apparent and intrinsic pK_as between MIF-wt and MIF-P1G calculated for the MD conformations. $\Delta pK_i = \Delta pK_i - wt - \Delta pK_i - P1G$. Likewise for ΔpK_a apparent.

Table I Experimental and Calculated pK_as of the N-Terminal Residue in the Wild-Type and Mutant Forms of Macrophage MIF[a]

PDB Code	pK_a ($\varepsilon_p = 20$)	pK_a^{int} ($\varepsilon_p = 20$)	pK_a ($\varepsilon_p = 4$)	pK_a^{int} ($\varepsilon_p = 4$)	pK_aExp[b]
Wild-type (1MIF)[c]	5.9	7.3	4.8	6.1	5.6–6.0
P1G (1P1G)[c]	5.1	6.0	3.6	4.1	< 5.5
P1A (1P1G)[d]	5.1	6.0	4.0	4.5	4.8
K32A (1MIF)[d]	7.4	7.4	6.4	6.5	6.8
Y95F (1MFF)[d]	6.5	7.4	6.1	6.2	6.3

[a] Experimental data from Refs. 14,16, and 46.
[b] Error associated to experimental pK_as is $\pm$ 0.1 unit.
[c] Standard deviation corresponding to calculated pK_as is 0.59 and 0.49 unit for wt and P1G, respectively. A total of 42 values were used to estimate each of these average pK_as.
[d] pK_a values were calculated for a single conformer (x-ray structures), and represent the average of the enzyme three active sites.

without necessarily causing a large atomic fluctuation of the glycine residue. Due the fact that this amino group plays a role in the proton transfer reaction and in keeping the ideal geometry and distance between base and acid during the reaction, it should in turn affect the catalytic efficiency of the MIF-P1G mutant.

CONCLUSIONS

We have carried out molecular dynamics and pK_a studies of MIF and its mutant P1G in order to investigate the origin of the lower catalytic efficiency of this mutation. Previously, two hypotheses have been proposed: (a) the lower basicity of primary amines, i.e., the N-terminal glycine with regard to the N-terminal proline; (b) the increased flexibility resulting from the replacement of a proline by a glycine.[20] We have found that in our MD simulations the N-terminal glycine does not display a particularly more flexible behavior with regard to proline. Instead, this glycine presents a larger accessibility to the solvent than the wild-type proline residue, which appears to disrupt the two hydrogen bonds involving its amine group and the residues Ala32 and Tyr36. Due to the key role of this amine group in the reaction catalyzed by MIF, we propose that the increased solvation of the N-terminal glycine with regard to the wild-type proline is the main cause for the lower catalytic efficiency of MIF-P1G.

JMB thanks Accelrys, Inc. (http://www.accelrys.com), for making the Insightll software and associated modules available to us through the Institute for Molecular Design at the University of Houston. Supercomputer time for this project was granted by NRAC to JMB and was made available on facilities at the San Diego Supercomputer Center. JMB also thanks the National Institutes of Health for support. TAS acknowledges the referees for insightful suggestions.

REFERENCES

1. David, J. R. Proc Natl Acad Sci USA 1966, 56, 72–77.
2. Bloom, B. R.; Bennett, B. Science 1966, 153, 80–82.
3. Bernhagen, J.; Calandra, T.; Mitchell, R. A.; Martin, S. B.; Tracey, K. J.; Voelter, W.; Manogue, K. R.; Cerami, A.; Bucala, R. Nature 1993, 365, 756–759.
4. Nishino, T.; Bernhagen, J.; Shiiki, H.; Calandra, T.; Dohi, K.; Bucala, R. Mol Med 1995, 1, 781–788.
5. Calandra, T.; Bernhagen, J.; Metz, C. N.; Spiegel, L.; Bacher, M.; Donnelly, T.; Cerami, A.; Bucala, R. Nature 1995, 377, 68–71.
6. Bacher, M.; Metz, C. N.; Calandra, T.; Mayer, K.; Chesney, J.; Lohoff, M.; Gemsa, D.; Donnely, T.; Bucala, R. Proc Natl Acad Sci USA 1996, 93, 7849–7854.
7. Rosengren, E.; Bucala, R.; Aman, P.; Jacobsson, L.; Odh, G.; Metz, C. N.; Rorsman, H. Mol Med 1996, 2; 143–149.
8. Rosengren, E.; Aman, P.; Thelin, S.; Hansson, C.; Ahlfors, S.; Bjork, P.; Jacobsson, L.; Rorsman, H. FEBS Lett 1997, 417, 85–88.
9. Subramanya, H. S.; Roper, D. I.; Dauter, Z.; Dodson, E. J.; Davies, G. J.; Wilson, K. S.; Wigley, D. B. Biochemistry 1996, 35, 792–802.
10. Sun, H. W.; Bernhagen, J.; Bucala, R.; Lolis, E. Proc Natl Acad Sci USA 1996, 93, 5191–5196.
11. Nishihira, J.; Fujinaga, M.; Kuriyama, T.; Suzuki, M.; Sugimoto, H.; Nakagama, A.; Tanaka, I.; Sakai, M. Biochemical and biophysical research communications 1998, 243, 538–544.
12. Johnson, W. H., Jr., Czerwinski, R. M.; Fitzgerald, M. C.; Whitman, C. P. Biochemistry 1997, 36, 15724–15732.
13. Stivers, J. T.; Abeygunawardana, C.; Mildvan, A. S; Hajipour, G.; Whitman, C. P. Biochemistry 1996, 35, 814–823.

14. Swope, M.; Sun, H. W.; Blake, P. R.; Lolis, E. EMBO J 1998, 17, 3534–3541.
15. Bendrat, K.; Al-Abed, Y.; Callaway, D. J. E.; Peng, T.; Calandra, T.; Metz, C. N.; Bucala, R. Biochemistry 1997, 36, 15356–15362.
16. Stamps, S. L.; Fitzgerald, M. C.; Whitman, C. P. Biochemistry 1998, 37, 10195–10202.
17. Soares, T. A.; Goodsell, D. S.; Briggs, J. M.; Ferreira, R.; Olson, A. J. Biopolymers 1999, 50, 319–328.
18. Stamps, S. L.; Taylor, A. B.; Wang, S. C.; Hackert, M. L.; Whitman, C. P. Biochemistry 2000, 39, 9671–9678.
19. Matsunaga, J.; Sinha, D.; Pannell, L.; Santis, C.; Wistow, G. J.; Hearing, V. J. J Biol Chem 1999, 274, 3268–3271.
20. Lubetsky, J. B.; Swope, M.; Dealwis, C.; Blake, P. R.; Lolis, E. Biochemistry 1999, 38, 7346–7354.
21. Anchell, J.; Apra, E.; Bernhold, D.; Borowski, P.; Clark, T. D.; Dachsel, H.; Deegan, M.; Dupuis, M.; Dyall, K.; Fann, G.; Fruchtl, H.; Gutowski, M.; Harrison, R.; Hess, A.; Jaffe, J.; Kendall, R.; Kobayashi, R.; Kutteh, R.; Lin, Z.; Littlefield, R.; Long, X.; Meng, B.; Nichols, J.; Nieplocha, J.; Stave, M.; Straatsma, T. P.; Taylor, H.; Thomas, G.; Wolinski, K.; Wong, A. NWChem, A Computational Chemistry Package for Parallel Computers, Version 3.1, High Performance Computational Chemistry Group, Pacific Northwestern National Laboratory, Richland, 1999.
22. Antosiewicz, J.; McCammon, J. A.; Gilson, M. K. J Mol Biol 1994, 238, 415–436.
23. Antosiewicz, J.; Briggs, J. M.; Elcock, A. H.; Gilson, M. K.; McCammon, J. A. J Comp Chem 1996, 17, 1633–1644.
24. Davis, M. E.; Madura, J. D.; Luty, B. A.; McCammon, J. A. Comp Phys Commun 1991, 62, 187–197.
25. Madura, J. D.; Briggs, J. M.; Wade, R. C.; Daves, M. E.; Luty, B. A.; Ilin, A.; McCammon, J. A. Comp Phys Commun 1995, 91, 57–95.
26. Berendsen, H. J. C.; Grigera, J. R.; Straatsma, T. P. J Comp Chem 1987, 91, 6269–6271.
27. Ryckaert, J. P.; Ciccotti, G.; Berendsen, H. J. C. J. Comp Phys 1977, 23, 327–341.
28. Mühlhahn, P.; Bernhagen, J.; Czisch, M.; Georgesku, J.; Renner, C.; Ross, A.; Bucala, R.; Holak, T. A. Protein Sci 1996, 5, 2095–2103.
29. Cornell, W. D.; Cieplak, P.; Bayly, C. I.; Gould, I. R.; Merz, K. M., Jr.; Ferguson, D. M.; Spellmeyer, D. C.; Fox, T.; Caldwell, J. W.; Kollman, P. A. J Am Chem Soc 1995, 177, 5179–5197.
30. Richards, F. M. Annu Rev Biophys Bioeng 1977, 6, 151–176.
31. Vriend, G. J Mol Graph 1990, 8, 52–56.
32. Davis, M. E.; McCammon, J. A. Chem Rev 1990, 90, 509–521.
33. Warwicker, J.; Watson, H. C. J Mol Biol 1982, 157, 671–679.
34. Helms, V.; Straatsma, T. P.; McCammon, J. A. J Phys Chem B 1999, 103, 3263–3269.
35. Branden, C.; Tooze, J. Introduction to Protein Structure; Garland Publishing: New York, 1999.
36. Hill, T. L. J Phys Chem 1956, 60, 253–255.
37. Rees, D. C. J. Mol Biol 1980, 141, 323–326.
38. Tanford, C.; Kirkwood, J Am Chem Soc 1957, 79, 5333–5339.
39. Gilson M. K.; Honig, B. Biopolymers 1986, 25, 2097–2119.
40. Smith P. E.; Brunne R. M.; Mark A. E.; van Gunsteren, W. F. J Phys Chem 1993, 97, 2009–2014.
41. Baptista A. M.; Soares, C. M. J Phys Chem B 2001, 105, 293–309.
42. Simonson, T.; Perahia, D.; Bricogne, G. J Mol Biol 1991, 218, 859–886.
43. Simonson T, Perahia D. PNAS 1995, 92, 1082–1086.
44. Demchuk, E.; Wade, R. C. J Phys Chem 1996, 100, 17373–17387.
45. Schaefer, M.; Sommer, M.; Karplus, M. J Phys Chem B 1997, 101, 1663–1683.
46. Grycuk T. J Phys Chem B 2002, 106, 1434–1445.
47. Johnson, W. H.; Czerwinski, R. M.; Stamps, S. L.; Whitman, C. P. Biochemistry 1999, 38, 16024–16033.
48. Soares, T. A.; Goodsell, D. S.; Ferreira, R.; Olson, A. J.; Briggs, J. M. J Mol Recognition 2000, 13, 146–156.
49. Hermann, R. B. J Comp Chem 1997, 18, 115–125.
50. Jackson, R. M.; Sternberg, J. E. Nature 1993, 366, 638–638.
51. Jackson, R. M.; Sternberg, J. E. Protein Eng 1994, 7, 371–383.
52. Hermann, R. B. J Phys Chem 1972, 76, 2754.
53. Eisenberg, D.; McLachlan, A. D. Nature 1986, 319, 199–203.
54. Honig, B.; Sharp, K.; Yang, A.-S. J Phys Chem 1993, 97, 1101–1109.
55. Funasaki, H.; Hada, S.; Neya, S.; Machida, K. J Phys Chem 1984, 88, 5786–5790.
56. Funasaki, H.; Hada, S.; Neya, S. J Phys Chem 1985, 89, 3046–3049.
57. Funasaki, H.; Hada, S.; Neya, S. J Med Chem 1983, 26, 686–693.
58. Serrano, L.; Neira, J.-L.; Sancho, J.; Fersht, A. R. Nature 1992, 356, 453–455.
59. Ooi, T.; Oobatake, M.; Nemethy, G.; Scheraga, H. A. Proc Natl Acad Sci USA 1987, 84, 3086–3090.
60. Ajay; Murcko, M. A. J Med Chem 1995, 38, 4953–4967.
61. Briggs, J. M.; Antosiewicz, J. In Lipkowitz, K. N.; Boyd, D. B. Eds; Reviews in Computational Chemistry; John Wiley & Sons: New York, 1999.
62. Taylor, A. B.; Czerwinski, R. M.; Johnson, W. H., Jr.; Whitman, C. P., Hackert, M. L. Biochemistry 1998, 37, 14692–14700.